Void reduction in fused filament fabrication (FFF) through *in situ* nozzle-integrated compression rolling of deposited filaments

Darshan Ravoori, Swapnil Salvi, Hardikkumar Prajapati, Momen Qasaimeh, Ashfaq Adnan & Ankur Jain

Published online: 17 Mar 2021.

Submit your article to this journal

View related articles

View Crossmark data

Taylor & Francis
Taylor & Francis Group

Check for updates

Void reduction in fused filament fabrication (FFF) through *in situ* nozzle-integrated compression rolling of deposited filaments

Darshan Ravoori, Swapnil Salvi, Hardikkumar Prajapati, Momen Qasaimeh, Ashfaq Adnan and Ankur Jain

Mechanical and Aerospace Engineering Department, University of Texas at Arlington, Arlington, TX, USA

ABSTRACT
The rastering of discrete polymer filaments during Fused Filament Fabrication (FFF) results in the formation of voids between filaments, leading to poor properties and performance of the printed part. Minimising voids and improving filament-to-filament adhesion remains a key technological challenge for FFF. While mechanical rolling is commonly used in traditional manufacturing, its use in polymer 3D printing has not been explored much. This paper discusses the *in situ* compression of just-deposited filament using a roller that is integrated with the filament-dispensing nozzle. The roller travels with the filament nozzle, and compresses the filament immediately after deposition when it is still soft. The rolling process is characterised using high speed imaging and infrared (IR) thermography. The effects of compression force and roller temperature on print quality is investigated. *In situ* compression of the filaments is shown to result in 10X reduction in void formation. Tensile test results show 154% improvement in Ultimate Tensile Stress (UTS) and 417% improvement in material toughness due to compressive rolling. It is expected that implementation of the rolling technique discussed in this work may help print parts with improved properties and functionality.

1. Introduction

Additive Manufacturing (AM) is widely used to manufacture parts with complicated geometries that are challenging to produce through conventional manufacturing methods. Typically, a three-dimensional geometry is sliced into multiple layers along the build direction, and the part is fabricated through layer-by-layer addition of material (Kruth, Leu, and Nakagawa 1998; Horn and Harrysson 2012; Wong and Hernandez 2012; Guo and Leu 2013). A number of different types of AM processes have been developed for both metal and polymer materials. A prominent polymer AM process is Fused Filament Fabrication (FFF), in which, a polymer wire is heated to above glass transition and dispensed through a rastering nozzle on top of previously deposited layers (Kruth, Leu, and Nakagawa 1998).

Poor thermal and mechanical properties of FFF-printed parts is a well-known challenge that must be overcome in order to produce functional parts that can withstand significant load (Hart et al. 2018; Goh et al. 2020a; Goh et al. 2020b). The directional nature of filament rastering and formation of voids between filaments is known to result in poor and anisotropic properties (Prajapati et al. 2018; Akhoundi and Behravesh 2019). Neck growth between neighbouring filaments (Bellehumeur et al. 2004; Sun et al. 2008; Seppala et al. 2017) is an important process during FFF that governs the mechanical strength of the printed part (Bellehumeur et al. 2004; Costa, Duarte, and Covas 2017). The rate of cooling of the interface temperature between two filaments layers plays a key role in polymer chain diffusion and neck growth – the slower the cooling, the more effective is the neck growth process. Poor adhesion and void formation may occur if the interface cools down too fast (Sun et al. 2008; Prajapati et al. 2018). The number and size of such voids greatly influence the mechanical properties of FFF-printed parts (Ang et al. 2006). Minimising voids during FFF remains a key technological challenge.

In view of the importance of minimising void formation, a number of studies have investigated the effect of process parameters such as print speed, layer width, print temperature, infill percentage and layer orientation on void formation and the resulting thermal and mechanical properties of printed parts (Prajapati et al. 2018), (Anitha, Arunachalam, and Radhakrishnan 2001; Ahn et al. 2002; Sood, Ohdar, and Mahapatra 2010; Tymrak, Kreiger, and Pearce 2014; Ning et al. 2017; Ravoori et al. 2018). The extent of void formation and resulting anisotropy in mechanical

properties has been investigated as a function of print speed and raster orientation (Ning et al. 2017). Tensile strength of the printed part has been correlated with layer height (Tymrak, Kreiger, and Pearce 2014). Maximum and minimum tensile strength were observed for raster angle of 0° and 90° respectively, which was explained on the basis of faster failure due to the load being imposed on the voids in the 90° case (Ahn et al. 2002).

Since void formation is intricately linked to the filament cooling process, a number of process modifications have been proposed to provide thermal energy in order to slow down filament cooling and reduce void formation. Nozzle-integrated *in situ* heating (Ravoori et al. 2019b), infrared (IR) heating (Kishore et al. 2017), microwave heating (Sweeney et al. 2017), laser heating (Ravi, Deshpande, and Hsu 2016) and hot air heating (Prajapati et al. 2020) are examples of such thermally-driven process modifications. However, these often consume significant energy and may have undesirable thermal side effects, such as material evaporation and internal microcrack generation (Ravi, Deshpande, and Hsu 2016). Post-fabrication thermal annealing has been shown to improve thermal (Prajapati et al. 2019) and mechanical (Hart et al. 2018) properties, but may be time-consuming and may cause significant warping.

In contrast to the thermally-driven methods discussed above, compression rolling of filaments may offer an attractive mechanism for reducing void formation in FFF, particularly if carried out while the filament is still hot and soft. The resulting flow of the viscous polymer may help fill voids between filaments. Hot and cold rolling are already well-established methods in conventional manufacturing such as metal (Groover 2010) and polymer (Bahadur 1975) processing. A high-pressure roller has also been used in metal AM to reduce longitudinal residual stress and even out the surface (Martina et al. 2015). While such an approach may also be effective for reducing void formation in polymer-based FFF, apart from the use of a pneumatically-actuated ring around the nozzle for compression (Love 2015; Duty et al. 2017), it has not been sufficiently reported in the literature. It is well-known that the interlaminar bond strength between neighbouring polymer filaments depends on processing temperature, processing time and applied pressure (Yang and Pitchumani 2002). Therefore, an *in situ* application of a carefully chosen amount of compressive load may reduce interlayer voids due to pressure-driven deformation of polymer filaments. Temperature may also play a key role in this process.

This paper presents a roller ball based technique to apply compression load on newly deposited filaments in conjunction with the filament deposition process. The roller balls are integrated to move along with the filament dispense nozzle, and thus provide *in situ* compression just after the filament is deposited. The temperature and pressure applied by the balls on the deposited filaments is independently controlled in an effort to reduce the fraction of voids and improve tensile strength of the printed part. High speed imaging and infrared thermography of the process is carried out while varying the ball weight, ball temperature and print speed. The impact of print speed and ball weight is investigated. Cross-section imaging of printed samples shows around 10X reduction in void percentage. Significant improvement in tensile properties is also reported. Amongst the process conditions studied, the greatest void reduction is found to be at a print speed of 2800 mm/min print speed and with the use of three balls, corresponding to a compression force of around 0.2 N based on ball weight. The technique discussed in this work offers a significant process improvement for FFF that may help improve the properties and function of printed parts.

2. Experiments

An experimental setup is designed and built to enable the application of compression load on newly deposited filament. A set of experiments are carried out to study the impact of *in situ* compression load on the filament mesostructure as well as properties of printed parts.

As shown in schematics and pictures in Figure 1, the compression load is applied on the filament by one or more roller balls contained in a roller barrel. The roller barrel is integrated with the nozzle assembly to move either ahead of (pre-nozzle configuration) or behind the nozzle (post-nozzle configuration). In practical printing conditions, since the nozzle travels in a U-pattern to print the next line, therefore, the position of the roller with respect to the nozzle changes from one line to the next. If the roller provides pre-deposition rolling in one line because of being ahead of the nozzle, it falls behind the nozzle while printing the next line, and therefore provides post-deposition rolling. In contrast, a dual-sided configuration with both pre- and post-nozzle rolling is also studied. Pictures and schematics of these configurations are shown in Figure 1. Sub-sections below describe the various elements of the experimental set up.

2.1. 3D printer setup

Most commercial desktop 3D printers provide limited access to the site of filament deposition for high speed
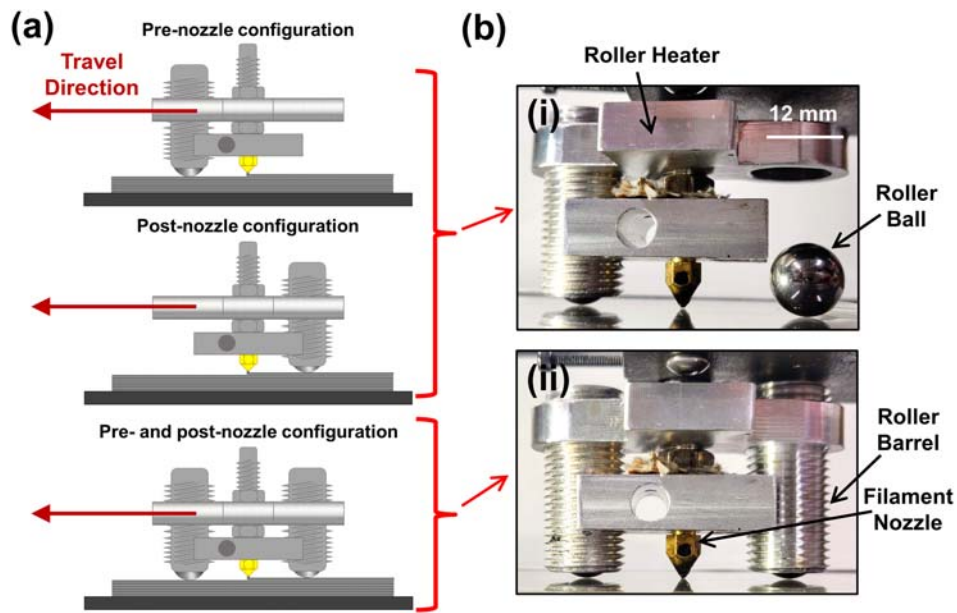
Figure 1. (a) Schematics of three configurations for filament compression rolling (not to scale); (b) Pictures of the roller barrel containing roller balls that is integrated with the moving filament nozzle. Both single-sided and dual-sided rollers are shown. The filament nozzle is shown in Yellow in (a). A small portion of the roller ball is seen protruding out of the roller barrel. A roller ball is also shown outside the barrel as an illustration.

imaging and infrared thermography. For this reason, in this work, an open source Anet A8 3D printer is used, which offers significant operational flexibility. The customised experimental setup is shown in Figure 2, with a zoom-in view of the nozzle roller assembly shown in Figure 1(b)(ii). A heated aluminum build plate of 200 mm by 200 mm size maintained at 60°C is used. An aluminum block is machined to accommodate the nozzle and barrel for polymer feed through. A 40 W resistive heater is embedded into the nozzle heater block along with a thermistor for temperature measurement. All experiments are carried out using Polylactic Acid (PLA) 1.75 mm filament (part number 3D PLA-1KG1.75-BLK from Hatchbox Inc., Ponoma, CA). For PLA, a recommended print temperature of 200°C is maintained by an A1284 mainboard based on feedback from thermistor. The nozzle diameter is 0.4 mm in all experiments. First layer height is set to 0.2 mm and is printed with a slower speed of 1000 mm/min to ensure good adhesion of the first layer with the print bed.

The *y* motion of the build plate, and *x* and *z* motions of the dispensing nozzle are controlled by stepper motors. Simplify3D software is used to convert the geometry of the part to be printed into G-code. The polymer feed rate is adjusted by the software based on the desired layer height and print speed. For baseline cases without roller compression, a layer height setting of 0.37 mm is used, per manufacturer recommendation. When the polymer is compressed by the ball roller, the

layer thickness may reduce, which may result in geometrical inaccuracy and build failure. In order to account for this, the layer height specific in the geometrical model is adjusted down by one percentage point per layer in order to account for the accumulative
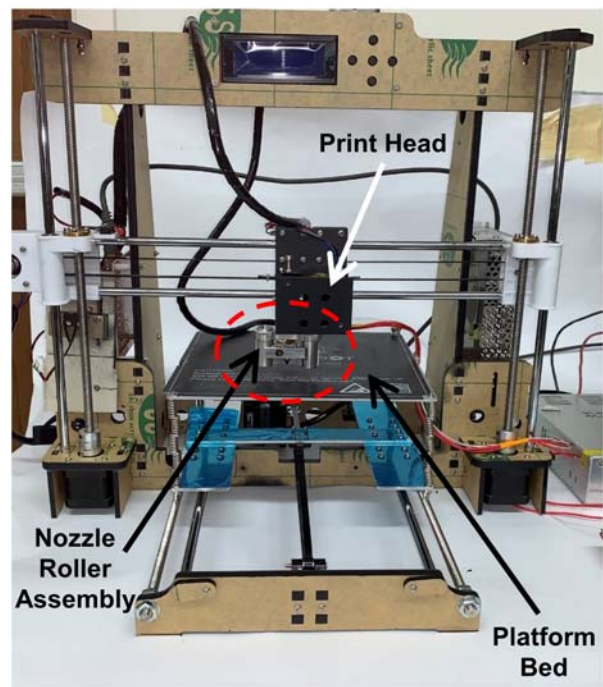

Figure 2. Picture of the experimental FFF setup. The nozzle roller assembly is highlighted. Zoom-in image of the nozzle roller assembly is shown in Figure 1(b)(ii).

compression as the layers build up. This one percentage point per layer adjustment is not necessarily optimal and needs to be investigated in more detail in order to result in the best possible printing results.

2.2. Integration of the metal ball roller with nozzle

Figure 1 presents schematics and pictures of pre-nozzle, post-nozzle as well as combined pre- and post-nozzle rolling arrangements. 12 mm diameter balls made up of 440C hardened bearing quality stainless steel (part number 1598K33, McMaster, Inc., Robbinsville, NJ) are used in experiments. Balls weigh 7 grams each, and are used to apply compression load due to ball weight on newly deposited filament. The nominal applied load due to ball weight is around 0.2 N for the three-ball configuration, although the force may vary somewhat due to friction between the ball and barrel surface. The use of bearing quality balls and slightly larger barrel size compared to ball diameter is expected to minimise friction and ensure rolling of the balls during printing. The area of contact between the spherical ball and barrel surface is likely to be small and also reduce friction. For illustration, one ball is shown outside the barrel in Figure 1(b). Spherical balls are used instead of a cylindrical roller for easier integration and ease of changing the compressive force by simply changing the number of balls. The balls are painted black for improving IR-based thermal measurements. The balls are contained in roller barrels that can be placed ahead of or behind the filament-dispensing nozzle (Figure 1(b)(i)) or both (Figure 1(b)(ii)). Each roller barrel can carry up to three balls. The entire assembly is designed such that the rolling ball is within 17 mm from the filament nozzle. As a result, the compression load is applied on the filament immediately after its deposition. This ensures that the filament temperature is still high, and viscosity is still low (Ravoori et al. 2019a) when the compression load is applied on the filament. Compressing with a roller at room temperature is likely to be ineffective, as it will result in rapid quenching of filament temperature. As a result, roller balls are heated, independent of the filament heater, using a 40 W resistive heater connected to each cylinder. In order to independently control the temperatures of the filament nozzle and roller balls, the nozzle heater surface is covered with thermal insulation. A thermistor is placed into the cylinder aluminum block to measure the barrel temperature and provide feedback to Arduino Mega 2560 circuit board. A wait time of around 20 minutes is implemented in order to reach thermal stability before starting experiments. The set temperature is specified to be slightly above the desired ball temperature in order to account for the small temperature differential that may exist between the barrel and balls. The ball temperature is verified before each experiment through an infrared camera measurement.

2.3. High speed visualisation and infrared temperature measurement

In situ high speed imaging and infrared thermography are carried out in order to understand the effect of the weight and temperature of the rolling ball on the deposited layers. These experiments are carried out with a FASTEC IL5SM4 high speed camera mounted to capture the side view of the polymer deposition process. A Navitar 12 V 150 W high intensity fibre optic light source is used for illumination. Image acquisition is carried out at 120 frames per second, with minimum 3 µs shutter time and 5 µm by 5 µm pixel size. White coloured PLA filament is used in these experiments for improving the quality of images. For these experiments, a thin, four-layer wall of 100 mm length is printed.

In addition to high speed imaging, infrared-based thermal measurements are also carried out to characterise the impact of roller temperature. A FLIR A6703sc InSb infrared camera operating in the 3.0–5.0 µm wavelength range is used for IR thrermography with a data capture rate of 30 frames per second. The infrared emission map measured by the camera is converted into a temperature map using a pre-calibrated value of emissivity. Black coloured filament is used in these experiments due to its higher emissivity, which is measured in advance using calibration experiments described in past work (Ravoori et al. 2019b). While two different colours of PLA are used in high speed visualisation and IR thermography experiments, past work (Wittbrodt and Pearce 2015) has indicated that there is no significant difference in the properties of Black and White PLA.

2.4. Void percentage measurement and tensile strength testing

Samples of dimensions 100 mm × 30 mm × 10 mm are printed and cross-sectioned in order to visualise the effect of compression rolling on void formation. The percentage of voids in the cross-section is measured quantitatively. In order to preserve the internal structure during the cross-sectioning process, a 0.5 mm cut is made at the centre of all edges of the sample, which is then immersed in liquid Nitrogen. Due to the resulting brittleness, the samples can be easily broken by an impact load to reveal the internal mesostructure of the sample, including voids, without distortion (Prajapati

et al. 2018; Prajapati et al. 2019; Ravoori et al. 2019b). Cross section images of these samples are taken with a 10 Megapixel AmScope microscope digital camera integrated with an AmScope 3X stereomicroscope. Void fraction is calculated using ImageJ software and correlated with process parameters.

Dogbone test coupons for tensile test measurements are printed, per modified version of ASTM D638-2a 'Standard Test Method for Tensile Properties of Plastics'. The test coupons are 74 mm long, 12 mm wide and 3.2 mm thick. Five samples each of baseline process and with rolling (3 ball weights of pre and post deposition rolling maintained at 110°C) are printed at a standard print speed of 60 mm/s. Two sets of test samples are printed. In the first sample, the print direction is aligned with the loading direction, i.e. the axis of the dogbone sample, so that the tensile load is applied along the direction of filaments. In the second sample, the print direction is normal to the loading direction, so that the load is applied normal to the filaments. Tensile testing is carried out using Shimadzu AGS-X series universal test frame with high precision 5 kN load cell and a pair of mechanical grips with a cross-head speed of 0.02 mm/min.

3. Results and discussion

A number of experiments are carried out in order to investigate the impact of roller pressure and temperature on the printing process as well as void fraction and tensile properties of printed parts. These experiments mainly examine the impact of two key process parameters – roller weight and roller temperature. The performance of pre-nozzle and post-nozzle rolling configurations is discussed in the next section. A combined dual-sided configuration containing both pre-nozzle and post-nozzle rolling is also discussed in section 3.3.

3.1. Effect of roller ball weight and temperature on layer height

3.1.1. Effect of roller ball weight at fixed temperature

The weight of the roller balls provides the compression load applied on the filament layer. The roller barrel can be loaded with up to three balls – the greater the number of balls, the higher is the load applied on the filament underneath. In order to understand the effect of compression load on the filament, high speed imaging is carried out for the printing process with the roller barrel loaded with one or three balls (Cases B and C). Results are compared with the baseline case without any compression load (Case A). In each case, the ball temperature is maintained at 110°C. Two

filaments of length 100 mm are deposited side-by-side and four such layers are printed in the z direction. Figure 3 shows images from each printing process at three different times during printing of the fourth layer. At $t = 0$ s, the polymer-dispensing nozzle is in view. At $t = 1.0$ s, the nozzle has travelled rightwards out of the frame, and the roller ball is seen compressing the deposited filament for Cases B and C. Once the nozzle and rolling ball pass away from the point of interest at $t = 1.7$ s, layer height is compared for all cases in order to determine the impact of the rolling process on layer height. Measurement of the layer height based on image analysis of the $t = 1.7$ s images indicates 10% & 17% reduction in layer height for one ball (Case B) and three balls (Case C) compared to the baseline.

There may be two distinct mechanisms behind the impact of the roller ball on the mesostructure of the filament layers. The first is a purely mechanical effect caused by filament compression due to the weight of the ball. The second is a thermal effect due to heat transfer to the filament from the hot ball. In order to understand the thermal impact of the roller ball, infrared thermography is carried out on the same process discussed above. Figure 4 shows successive images for the case of compression rolling with three balls at 110°C starting at $t = 0$ s when the filament deposition occurs. The hot roller ball is clearly visible in Figure 4 at $t = 1.0$ s. However, Figure 4 also shows that the thermal impact of the roller ball is rather localised in time. Figure 4 shows that the temperature distribution for the roller case returns close to the baseline very quickly after the ball rolls over the point of interest. This is consistent with the short duration of contact between the ball and filament, as well as the small area of contact expected between the two, which limits the extent of heat transfer between the two.

Temperature data are extracted from the thermal images in Figure 4 and plotted. Figure 5 plots temperature of the weld interface between the third and fourth layers as a function of time for the baseline case as well as printing with one, two and three roller balls. In this plot, $t = 0$ corresponds to the time at which nozzle deposits the fourth filament layer at the point of interest. The cooling curves are nearly the same for each case, except for a small peak around $t = 1.0$ s, when the roller moves past the point of interest. The inset in Figure 5 zooms into the period around $t = 1.0$ s. It is seen that the greater the number of balls, the larger is the bump. However, the temperature profile very quickly returns to match the baseline case. The weld quality between layers depends on the temperature history (Pokluda, Bellehumuer, and Vlachopoulos 1997; Yang and Pitchumani 2002). However, the temperature bump shown in Figure 5
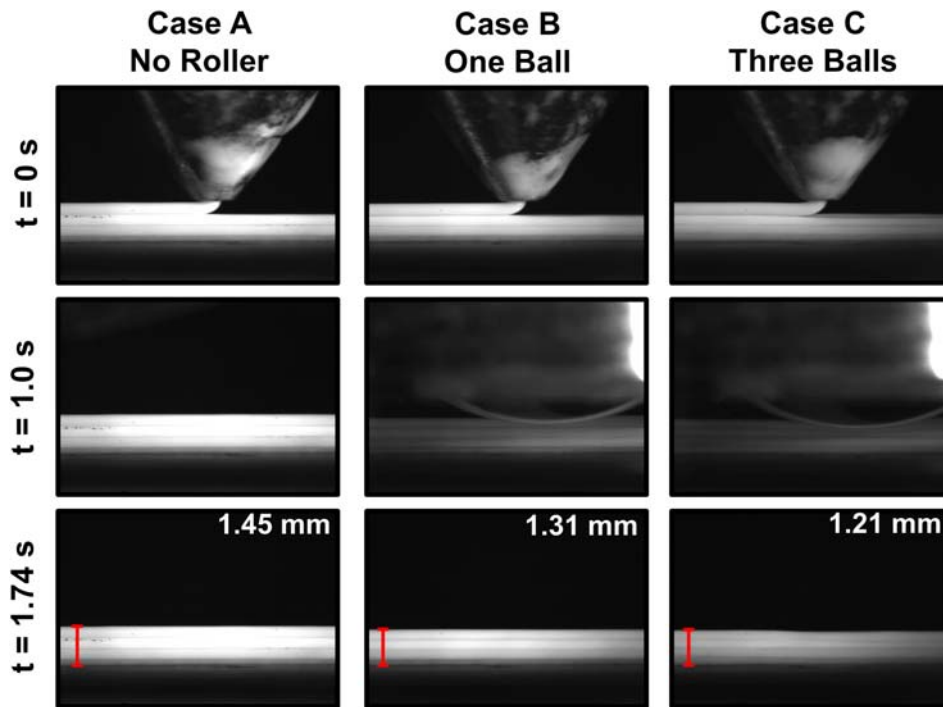
Figure 3. Successive high speed images for three cases to investigate the effect of compression load on the filament thickness. Numbers shown in the last set of images are the final thicknesses of the four-layer printed part. The roller balls are maintained at 110°C in Cases B and C. The print speed is 3600 mm/min.

is small and short-lived, and the temperature integral does not change by more than 1% for each case compared to baseline. Therefore, the significant adhesion improvement obtained here can not be attributed to temperature rise. Instead, the reduction in total height as seen in Figure 3 is mostly attributable to the mechanical compression of the filament due to the roller ball.

Note that for large area printing, the impact of rolling may be limited because the previously-deposited filament may cool down significantly before the roller returns to apply the compressive load. In such a case, rolling may need to be supplemented with directed heat supply to the filament, such as through *in situ* heating (Ravoori et al. 2019b) or external energy
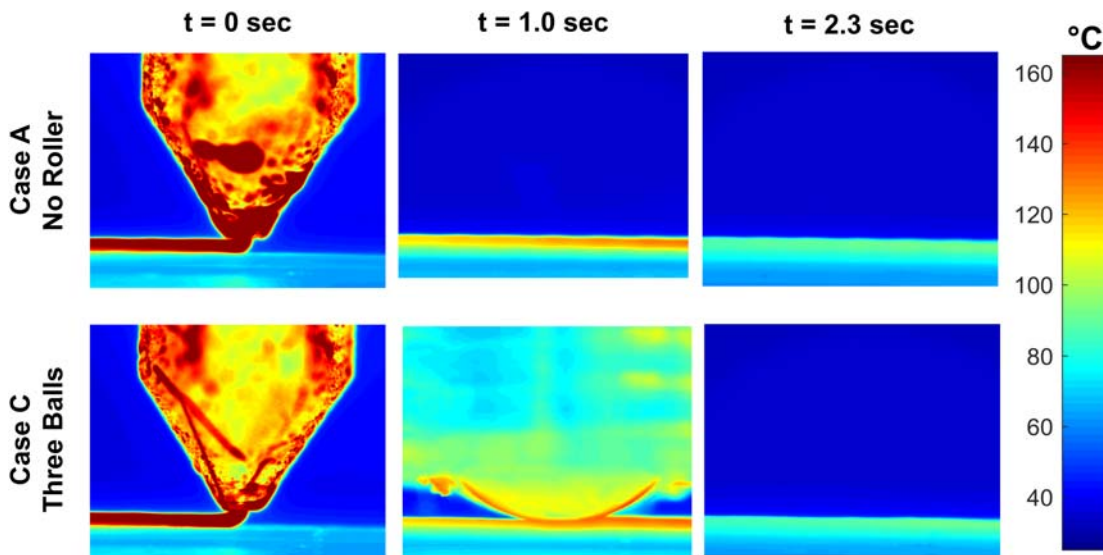

Figure 4. Infrared-based temperature maps of the printing process comparing the baseline case with no roller (Case A) with the three roller ball case (Case C).
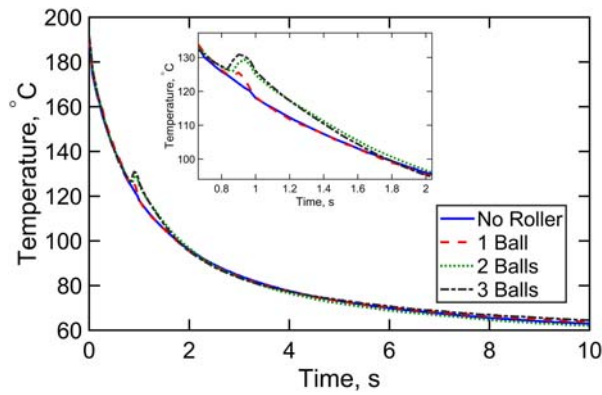
Figure 5. Post-deposition temperature decay profile for a filament with compression rolling with different number of balls. The baseline case is also shown for comparison.

sources (Ravi, Deshpande, and Hsu 2016; Kishore et al. 2017; Sweeney et al. 2017).

3.1.2. Effect of roller ball temperature at fixed weight

The roller ball temperature may be an important parameter because if the ball temperature is too low, it may cause undesirable cooling down of the filament when it comes in contact with the roller ball. On the other hand, too high a roller temperature may cause uneven layer height and adhesion of the polymer to the ball. In order to investigate this aspect further, experiments are carried out at three different roller ball temperatures – 90, 110 and 160°C – and compared with the

baseline no-roller case. In each case, three balls are loaded in the barrel in order to maintain the same compression load. All other print process conditions are the same as for Figures 3 and 4. Figure 6 compares high speed images for these cases with the baseline case of zero compression. As the roller ball temperature increases, there is progressively greater reduction in layer height since the filament is softer at higher temperatures. However, at high roller ball temperatures, the deposited polymer sticks back to the moving roller ball, as seen in the last column for 160°C ball temperature in Figure 6. This is undesirable, as it results in uneven layer height and part build failure. For this case, small fragments of polymers are found to be stuck on the roller ball after completion of the printing process.

3.2. Void fraction measurement

Void fraction measurements are carried out on samples printed with roller ball compression for comparison with baseline parts. The parts printed for this purpose are much larger than the ones used in the previous section. The overall part size is 100 mm × 30 mm × 10 mm, with a print orientation of 0° and roller configuration similar to the one shown in Figure 1(b)(i). During the print process, the nozzle moves back and forth along the 100 mm long *x* direction. As a result, in one pass, the roller provides pre-deposition compression when it moves ahead of the nozzle and in the next pass after a U-turn, it provides post-deposition
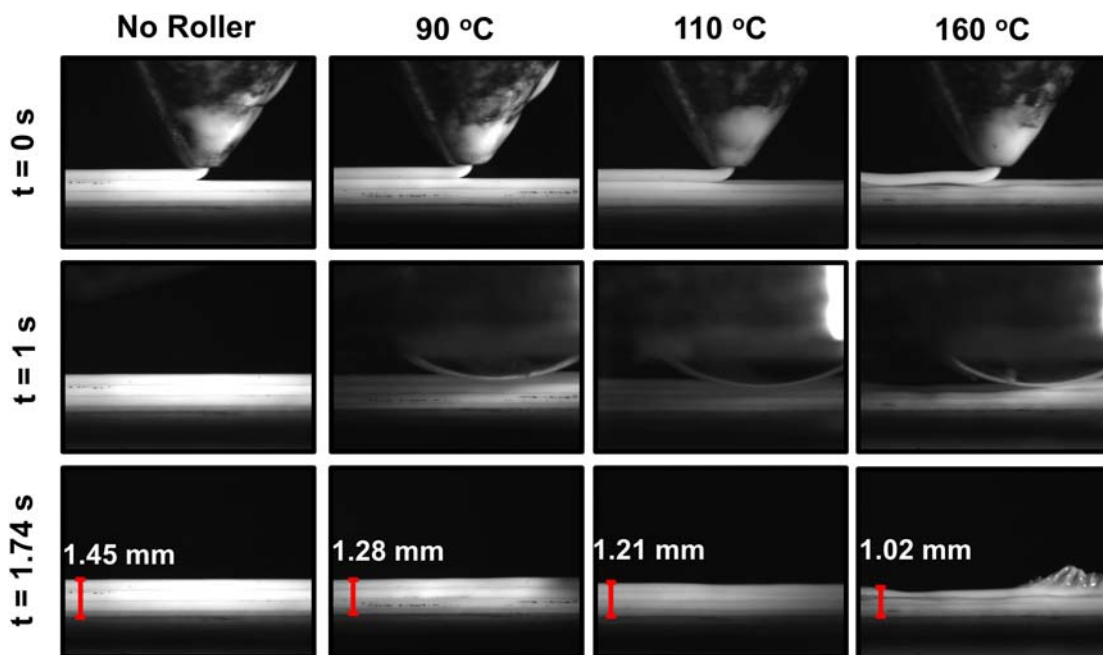

Figure 6. Successive high speed images for three different values of the roller ball temperature. Numbers shown in the last set of images are the final thickness of the four-layer printed part. Three roller balls are used in each case, and the print speed is 3600 mm/min.

compression because it now moves behind the nozzle. Samples are printed with either one or three roller balls, and at three different speeds – 2000, 2800 and 3600 mm/min – in addition to the baseline case. Note that 3600 mm/min is the optimal, manufacturer-recommended print speed. The roller balls are maintained at 110°C in each case. Three replicates of samples are printed for each test case. The samples are cross-sectioned and void fraction is measured following the process described in section 2.4.

Figure 7 shows sample cross-sections for one and three ball cases for three different print speeds. These cross-section images clearly show improved neck growth and reduced voiding for both one-ball and three-ball cases compared to the baseline. There is somewhat better performance for the three-ball case, which is consistent with the layer height measurements shown in the high speed images in Figure 3. The baseline images for 2000 mm/min speed show poor contact between layers, which is because the speed is much lower than the manufacturer-recommended setting of 3600 mm/min.

The intermediate speed of 2800 mm/min appears to perform slightly better than the other two speeds in terms of void fraction reduction. This can be qualitatively explained as follows: At too low a speed, a large time passes before the roller reaches the deposited filament, by when, the filament has already cooled down significantly, thereby limiting the impact of the rolling process. On the other hand, at too high a speed, the filament experiences the compression load over a very short time, which also limits the impact of the rolling process. An intermediate speed is, therefore, likely to be optimal. The optimal speed can possibly be tuned by changing the distance between the filament nozzle and the roller. For example, bringing the two closer to each other will ensure that the deposited filament is still hot enough when the roller comes in contact. The optimal speed is also likely a function of the properties of the polymer.

Figure 8(a) and (b) plot the average void percentage over three replicates as a function of print speed and ball weight for one-ball and three-ball cases, respectively. Three temperatures – 90°C, 100°C and 110°C – are used. Note that the 160°C case is excluded from Figure 8 because it leads to poor part quality due to polymer sticking to the ball and uneven layer height, as shown in Figure 6. Figure 8 shows significant
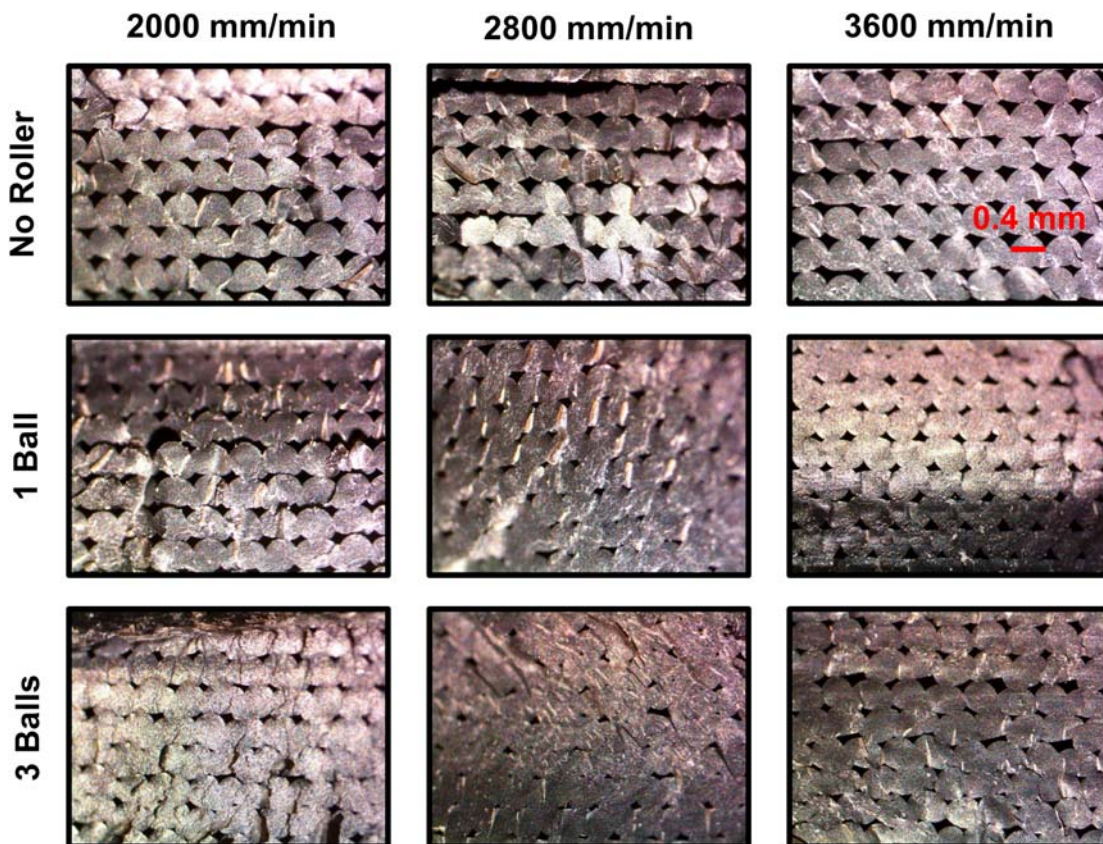

Figure 7. Cross-sections of parts printed at three different print speeds and with 0, 1 and 3 balls for compression rolling. The ball temperature is 110°C for each case. Images from the baseline process are also shown for comparison.
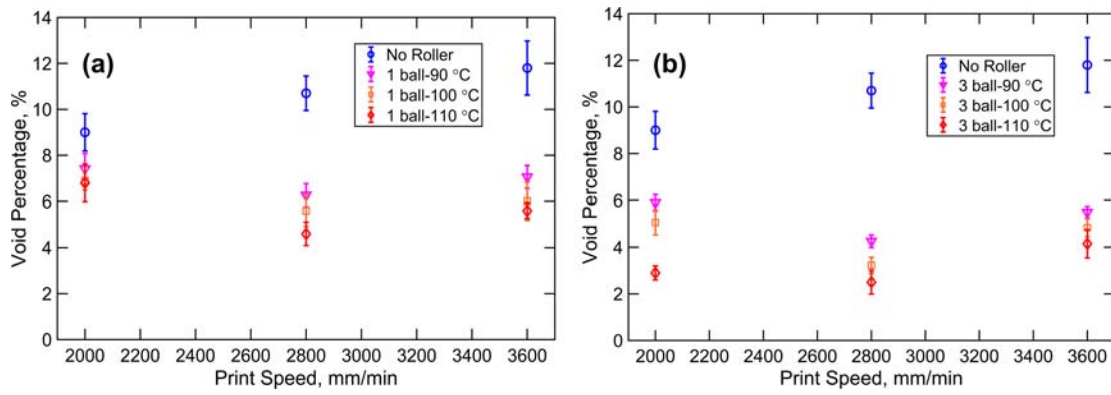
Figure 8. Void percentage for single-sided rolling as a function of print speed and roller ball temperature for (a) one ball and (b) three ball cases.

reduction in void fraction for all compression rolling cases compared to the no-roller baseline. In general, the three-ball case offers greater improvement than the one-ball case. The best performance is seen for the ball temperature of 110℃ and print speed of 2800 mm/min, although other cases are also quite close. For this case, the void fraction for the three-ball and one-ball experiments are 2.5% and 4.5%, respectively, which represents a significant improvement compared to the baseline value of 10.8%. Note that the 2000 mm/min print speed is much lower than the manufacturer-recommended setting, and, therefore, care must be taken when comparing baseline and roller samples at this speed.

3.3. Dual-sided rolling

In contrast to the pre-nozzle or post-nozzle compression presented so far, an alternate approach of providing dual-sided rolling is also investigated. In this case, as shown in Figure 1(b)(ii), two roller barrels are integrated on both sides of the rastering nozzle, so that pre-nozzle and post-nozzle compression are both provided simultaneously. These experiments are carried out with roller ball temperature of 110℃ and standard print speed of 3600 mm/min. High speed imaging of this process shows a 21% reduction in layer height due to the dual rolling compared to the baseline, which is slightly greater than the 16% reduction seen for the single-sided rolling discussed in Figure 4.

Figure 9 shows cross-sections images for void characterisation of the dual-sided rolling approach. The improvement in voiding due to dual-sided rolling is clearly seen when compared to the baseline. The improvement is even greater than in the single-sided rolling case (Figure 7). Figure 10 plots the void percentage as a function of print speed and ball temperature for one ball and three ball cases. These images and

void percentage data show that there is even greater improvement in void formation for the dual-sided rolling compared to the single-side rolling case. For 2800 mm/min print speed with three rolling balls, the void fraction reduced to only 0.7% compared to the baseline value of 10.8%, which is a significant improvement that nearly eliminates voids.

3.4. Impact of overall geometrical dimensions

Since the roller ball causes mechanical compression of the filament, it is important to ensure that this technique does not result in distortion of the overall geometrical dimensions of the printed part. In order to characterise this effect, a standard parallelepiped sample is printed with three-ball roller compression with a ball temperature of 110℃. As a baseline, the sample is also printed without roller compression. In both cases, the print speed is 2800 mm/min. The overall geometrical dimensions of the printed parts is measured and summarised in Table 1.

Data in Table 1 show that geometrical distortion occurs primarily in the build direction only, which is not surprising, since the compression load is applied in that direction. The key reason behind distortion in the build direction is that the CAD model of the sample did not take into account the dimensional reduction caused by the compression roller. While the reduction in voiding due to compression roller is certainly desirable, steps also need to be taken to minimise the resulting impact on geometrical accuracy of the printed part. One possible way to ensure this is to simply revise the CAD model dimensions upwards in order to counteract the expected reduction. While this simplistic approach is found to work well for simple parts such as ones printed here, further research is needed for fully understanding and implementing such a correction in parts with more complicated geometry. This will help retain
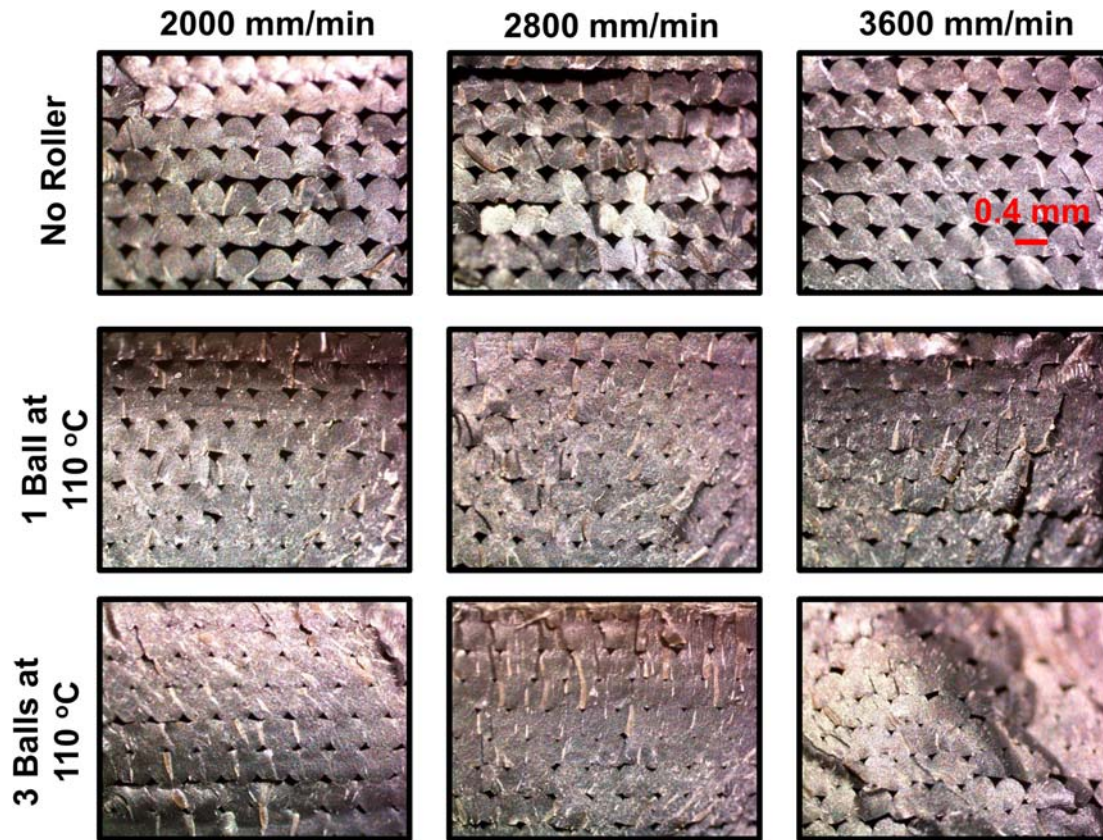
Figure 9. Cross-sections of parts printed with dual-sided rolling. Images are shown for one-ball and three-ball cases with three different print speeds. The ball temperature is 110°C for each case. Images from the baseline process are also shown for comparison.

the beneficial effect of void reduction through compression rolling while preserving the geometrical accuracy of the printed part.

3.5. Tensile tests

The impact of compression rolling of filaments on mechanical properties of printed parts is investigated through tensile testing. It is expected that the void reduction seen in Figures 7–10 will result in improved tensile properties. Two distinct sets of samples are printed at the manufacturer-recommended speed of 3600 mm/min to investigate the impact on tensile properties. In Sample A, the filaments are printed along the same direction as the direction of application of the tensile load (0° angle between the print direction and the load direction, which is the axis of the dogbone sample). The stress–strain curve for this sample is shown in Figure 11. All
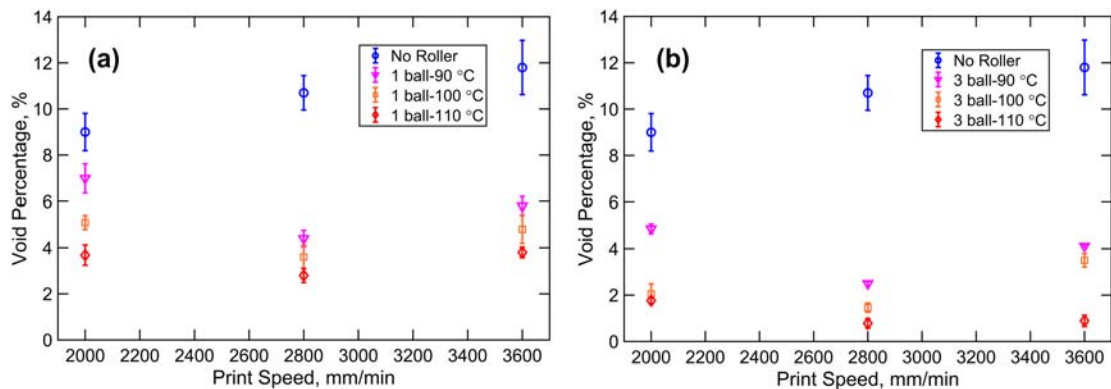

Figure 10. Void percentage for dual-sided printing as a function of print speed and roller ball temperature for (a) one ball and (b) three ball cases.

Table 1. Comparison of overall geometrical dimensions of baseline and rolled parts.

X (Raster Direction)			Y			Z (Build Direction)		
Baseline (mm)	Rolled (mm)	% change	Baseline (mm)	Rolled (mm)	% change	Baseline (mm)	Rolled (mm)	% change
80.3	80.7	+0.50	9.9	10.1	+1.98	8.1	6.44	−20.5
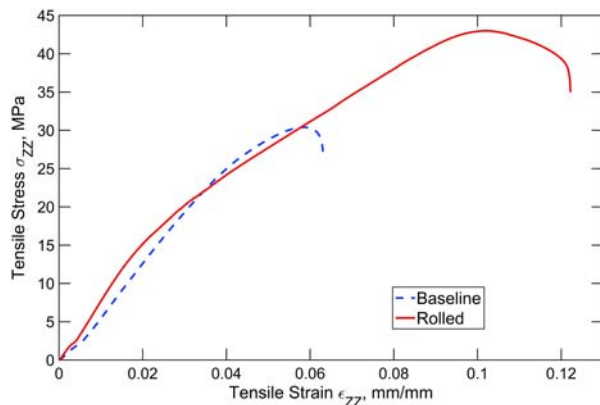
Figure 11. Stress-strain curve from tensile testing of Sample A printed with the print direction aligned with the loading direction. Performance of a sample printed with dual-sided rolling is compared with a baseline sample with no compression rolling.

results from tensile tests are summarised in Table 2. Compared to baseline, data show 34% improvement in Ultimate Tensile Stress (UTS) and 281% improvement in material toughness. The second test is carried out on Sample B, in which, the tensile load is applied normal to the print direction (90° angle between the print direction and load direction). Data for Sample B, shown in Figure 12 and Table 2, demonstrate even greater improvement in tensile properties – a 149% improvement in UTS, and 495% improvement in material toughness. A t-test of the measurements for both ultimate tensile stress and toughness shows that for both Samples A and B, the reported improvements are statistically significant ($p < 0.001$).

The fracture surfaces for the rolled samples appear to be different from the baseline samples, in both cases investigated here (i.e. when the printing direction is aligned with or normal to the load direction). It is believed that the failure process is governed by crazing, and presence of crazing is more pronounced on the fracture surface of the rolled coupons. Necking before fracture is observed during tensile testing, which is also discernible from the stress–strain curves of the rolled samples. The presence of crazing in the rolled samples also supports the increase in material toughness.

It is expected that rolling on the just-deposited filaments while still hot and soft deforms the filaments in the lateral direction, thereby filling gaps between filaments, improving interfacial bonding and reducing void formation. The reduced gap between filaments is clearly seen in cross-section images in Figures 7 and 9. Rolling also works to reshape the filaments, resulting in increasing the notch angle at the interface. Rolling may also help improve the singularity order, which results in enhancing the material toughness (Rezaee and Adnan 2018), as is evident in Figure 12. Tensile toughness of a material is described by the ability of the material to absorb tensile fracture energy during stretching. For PLA, tensile toughness can be increased through two distinct mechanisms –shear yielding and crazing energy (Zhao et al. 2020). Of these, shear yielding is the most effective mechanism for significant change in toughness. As evident from the tensile stress–strain curves, it is believed that the rolling process and temperature collectively rearrange the internal molecular structure of PLA, which, in turn, enhances plasticity (shear yielding) in the material. In addition, rolling may also help align polymer chains along the printing direction, which may also have contributed towards the improved UTS when loaded along the filament direction (Bahadur 1975), as shown in Figure 11.

A comparison between Figures 11 and 12 shows that the UTS values are very similar for Samples A and B that are printed/rolled along and normal to the loading directions, respectively. In contrast, UTS of the baseline sample with 90° angle between printing and loading directions is much lower – nearly half – than that of

Table 2. Comparison of tensile test properties of compression-printed parts with baseline parts. Data are presented for two samples that are printed along with or normal to the load direction.

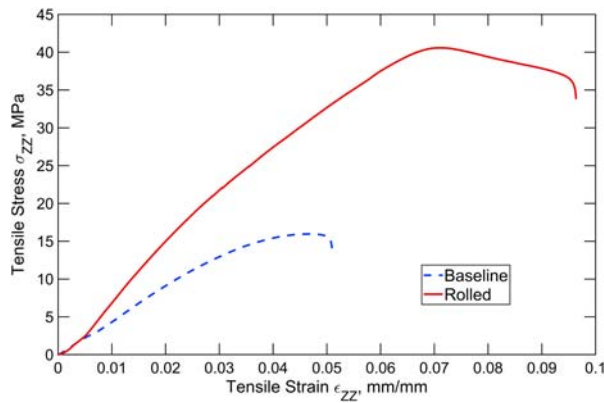|	Description	Ultimate strength (MPa)	Increase in ultimate tensile strength, %	Toughness (MJ/m^3)	Increase in toughness, %
Sample A	Baseline	33.3 ± 2.4	34%	1.1 ± 0.2	281%
	Compressive Rolling aligned with tensile load direction	44.7 ± 1.5		4.2 ± 0.8	
Sample B	Baseline	15.5 ± 0.9	149%	0.4 ± 0.05	495%
	Compressive Rolling normal to tensile load direction	38.6 ± 1.8		2.6 ± 0.3	

Figure 12. Stress-strain curve from tensile testing of Sample B printed with the print direction normal to the loading direction. Performance of a sample printed with dual-sided rolling is compared with a baseline sample with no compression rolling.

the baseline sample with 0 degrees loading angle. This indicates that the compressive load due to rolling is likely resulting in improved interdiffusion of polymer chains, and thereby, a better degree of healing (Yang and Pitchumani 2002). While more theoretical modelling may be needed to completely characterise the impact of compression rolling on the polymer interdiffusion process, data presented here indicate that hot rolling of filaments may help address two key challenges in the 3D printing process – the degree of anisotropy in tensile properties, and the weakness of 3D printed parts under transverse loading.

5. Conclusions

Improvement in filament-to-filament adhesion and reduction in void formation are key technological challenges in enabling polymer FFF to print functional parts. This work shows that compressive rolling of just-deposited filaments may be an effective technique for addressing this challenge. Despite not optimising the rolling process much, this work demonstrates significant reduction in void formation from 10.8% to less than 1%, as seen in cross-section images, and corresponding improvement in mechanical properties, as evident from tensile test results.

It is interesting to note the key advantages of the present approach over other, thermally-driven approaches for filament adhesion improvement reported in the past. The present approach is a non-thermal one, and therefore, it avoids collateral thermal damage in the vicinity of the filament, such as development of micro-cracks. The present approach consumes minimal energy, and is passive, in that it does not need to be actively controlled. Finally, changing the compression load, which

may be necessary when working with different polymers, can be achieved easily by changing the number of balls or replacing with balls of a different weight.

It is important to recognise that the roller technique described here changes the layer height due to compression, and the overall height of the printed part may also be affected. There is a need to optimally determine the layer height setting that accounts for the compression effect. In experiments with the roller, using a constant layer height is found to be ineffective, because the layer compression grows as layers build. A layer height setting with gradual reduction in layer height is found to result in good printing. However, this is not necessarily optimal and more work is needed to fully establish the impact of roller compression on layer height setting. This may require mechanical simulations of the compression process, combined with experimental data and machine learning (Baumann et al. 2018; Meng et al. 2020).

Note that the optimal rolling temperature and compressive loading obtained in this work are specific to PLA filament, as these parameters are likely to depend strongly on the filament properties. For other filament materials, these parameters may need to be determined through separate experiments. Further note that in the present work, the roller is in continuous contact with the part being printed. In case continuous contact is not desired, for example, when printing support structures, it may be possible to design an electromagnetic or spring-based actuator to turn the roller action on/off by lifting the balls above the part being printed.

It is expected that further optimisation, such as by changing the filament-roller distance, as well as the use of other compression modes such as cylindrical roller instead of spherical balls, may further improve the print quality. The process of *in situ* filament compression by rolling at a temperature above the material's glass transition temperature can be further studied via theoretical modelling that combines aspects of heat transfer, applied mechanics and polymer physics. Such a theoretical understanding of this process may drive further process optimisation. Finally, it may be interesting to investigate the applications of this work for large area additive manufacturing, where the large print size offers unique challenges. For example, for large prints, the pre-deposited layer will cool down and be close to surrounding environment temperature before the pre-deposition roller arrives, thereby limiting the impact of the pre-roller. In such a case, the printing may need to be carried out in a thermally controlled environment, or with nozzle-integrated *in situ* heaters (Ravoori et al. 2019b) in order to fully utilise the benefit of roller compression.

Disclosure statement

Funding

Notes on contributors

Darshan Ravoori completed his PhD in Mechanical Engineering from the University of Texas at Arlington, where he carried out research on measurements and modeling of polymer 3D printing processes. At present, he works at Intel Corporation.

Swapnil Salvi is pursuing his PhD in Mechanical Engineering from the University of Texas at Arlington. His research interests include heat transfer measurements, infrared thermography and additive manufacturing.

Hardikkumar Prajapati completed his PhD in Mechanical Engineering from the University of Texas at Arlington, where he carried out research on measurements and optimization of polymer 3D printing processes. At present, he works at Intel Corporation.

Momen Qasaimeh is pursuing his PhD in Mechanical Engineering from the University of Texas at Arlington. His research interests include additive manufacturing and thermomechanical simulations.

Ashfaq Adnan is a Professor in the Mechanical & Aerospace Engineering Department and director of the Multiscale Mechanics and Physics Lab (MMPL). He earned his PhD in Aeronautics & Astronautics Engineering from Purdue University. He is an ASME fellow and the recipient of 2020 Lockheed Martin Teaching Award.

Ankur Jain is an Associate Professor in the Mechanical and Aerospace Engineering Department at the University of Texas at Arlington. He has published 87 journal papers on topics related to theoretical and applied heat transfer, including in additive manufacturing, batteries and microelectronics. He is a recipient of the NSF CAREER Award in 2016, UT Arlington College of Engineering Outstanding Early Career Award in 2017 and Lockheed Martin Aeronautics Excellence in Teaching Award in 2018. He received his Ph.D. from Stanford University in 2007.

Data availability statement

The data that support the findings of this study are available from the corresponding author upon reasonable request.

Credit authorship contribution statement

D. Ravoori – Methodology, Investigation, Visualisation, Data Curation; S. Salvi – Methodology, Investigation, Visualisation, Data Curation; H. Prajapati – Investigation, Visualisation; M. Qasaimeh – Investigation; A. Adnan – Methodology, Supervision; A. Jain – Conceptualisation, Methodology, Supervision, Project Administration. All authors contributed towards Writing Original Draft, Review and Editing.

References

Ahn, S., M. Montero, D. Odell, S. Roundy, and P. K. Wright. 2002. "Anisotropic Material Properties of Fused Deposition Modeling ABS." *Rapid Prototyping Journal* 8: 248–257.

Akhoundi, B., and A. H. Behravesh. 2019. "Effect of Filling Pattern on the Tensile and Flexural Mechanical Properties of FDM 3D Printed Products." *Experimental Mechanics* 59 (6): 883–897.

Ang, K. C., K. F. Leong, C. K. Chua, and M. Chandrasekaran. 2006. "Investigation of the Mechanical Properties and Porosity Relationships in Fused Deposition Modelling-Fabricated Porous Structures." *Rapid Prototyping Journal* 12: 100–105.

Anitha, R., S. Arunachalam, and P. Radhakrishnan. 2001. "Critical Parameters Influencing the Quality of Prototypes in Fused Deposition Modelling." *Journal of Materials Processing Technology* 118: 385–388.

Bahadur, S. 1975. "The Effect of Hot and Cold Rolling on the Properties of Poly(Oxymethylene)." *Polymer Journal* 7: 613–621.

Baumann, F., A. Sekulla, M. Hassler, B. Himpel, and M. Pfeil. 2018. "Trends of Machine Learning in Additive Manufacturing." *International Journal of Rapid Manufacturing* 7: 310–336.

Bellehumeur, C., L. Li, Q. Sun, and P. Gu. 2004. "Modeling of Bond Formation Between Polymer Filaments in the Fused Deposition Modeling Process." *Journal of Manufacturing Processes* 6: 170–178.

Costa, S. F., F. M. Duarte, and J. A. Covas. 2017. "Estimation of Filament Temperature and Adhesion Development in Fused Deposition Techniques." *Journal of Materials Processing Technology* 245: 167–179.

Duty, C., V. Kunc, B. Compton, B. Post, D. Erdman, R. Smith, R. Lind, P. Lloyd, L. Love. 2017. "Structure and Mechanical Behavior of Big Area Additive Manufacturing (BAAM) Materials." *Rapid Prototyping Journal* 23: 181–189.

Goh, G. D., V. Dikshit, J. An, and W. Y. Yeong. 2020a. "Process-Structure-Property of Additively Manufactured Continuous Carbon Fiber Reinforced Thermoplastic: An Investigation of Mode I Interlaminar Fracture Toughness." *Mechanics of Advanced Materials and Structures*, 1–13. https://doi.org/10.1080/15376494.2020.1821266

Goh, G. D., Y. L. Yap, H. K. J. Tan, S. L. Sing, G. L. Goh, and W. Y. Yeong. 2020b. "Process–Structure–Properties in Polymer Additive Manufacturing via Material Extrusion: A Review." *Critical Reviews in Solid State and Materials Sciences* 45 (2): 113–133.

Groover, M. 2010. *Fundamentals of Modern Manufacturing: Materials, Processes, and Systems*. 4th ed. New York, NY: Wiley.

Guo, N., and M. C. Leu. 2013. "Additive Manufacturing: Technology, Applications and Research Needs." *Frontiers of Mechanical Engineering* 8: 215–243.

Hart, K. R., R. M. Dunn, J. M. Sietins, C. M. H. Mock, M. E. Mackay, and E. D. Wetzel. 2018. "Increased Fracture Toughness of Additively Manufactured Amorphous Thermoplastics via Thermal Annealing." *Polymer* 144: 192–204.

Horn, T. J., and O. L. A. Harrysson. 2012. "Overview of Current Additive Manufacturing Technologies and Selected Applications." *Science Progress* 95: 255–282.

Kishore, V., C. Ajinjeru, A. Nycz, B. Post, J. Lindahl, V. Kunc, and C. Duty. 2017. "Infrared Preheating to Improve Interlayer Strength of Big Area Additive Manufacturing (BAAM) Components." *Additive Manufacturing* 14: 7–12.

Kruth, J. P., M. C. Leu, and T. Nakagawa. 1998. "Progress in Additive Manufacturing and Rapid Prototyping." *CIRP Annals* 47 (2): 525–540.

Love, L. 2015. "Cincinnati Big Area Additive Manufacturing." Technical Report NFE-14-04957, Oak Ridge National Laboratory. Available at https://info.ornl.gov/sites/publications/files/Pub54708.pdf, last accessed January 18, 2021.

Martina, F., P. Colgrove, S. Williams, and J. Meyer. 2015. "Microstructure of Interpass Rolled Wire + Arc Additive Manufacturing Ti-6Al-4V Components." *Metallurgical and Materials Transactions A* 46: 6103–6118.

Meng, L., B. McWilliams, W. Jarosinski, H-Y. Park, Y-G. Jung, J. Lee, and J. Zhang. 2020. "Machine Learning in Additive Manufacturing: A Review." *JOM Journal of the Minerals Metals and Materials Society* 72: 2363–2377.

Ning, F., W. Cong, Y. Hu, and H. Wang. 2017. "Additive Manufacturing of Carbon Fiber-Reinforced Plastic Composites Using Fused Deposition Modeling: Effects of Process Parameters on Tensile Properties." *Journal of Composite Materials* 51: 451–462.

Pokluda, O., C. Bellehumeur, and J. Vlachopoulos. 1997. "Modification of Frenkel's Model for Sintering." *AIChE Journal* 43: 3253–3256.

Prajapati, H., D. Chalise, D. Ravoori, and A. Jain. 2019. "Improvement in Build-Direction Thermal Conductivity in Extrusion-Based Polymer Additive Manufacturing Through Thermal Annealing." *Additive Manufacturing* 26: 242–249.

Prajapati, H., D. Ravoori, R. Woods, and A. Jain. 2018. "Measurement of Anisotropic Thermal Conductivity and Inter-Layer Thermal Contact Resistance in Polymer Fused Deposition Modeling (FDM)." *Additive Manufacturing* 21: 84–90.

Prajapati, H., S. S. Salvi, D. Ravoori, M. Qasaimeh, A. Adnan, and A. Jain. 2020. "Improved Print Quality in Fused Filament Fabrication Through Localized Dispensing of Hot Air Around the Deposited Filament." *Additive Manufacturing*, 40: 101917:1–9.

Ravi, A., A. Deshpande, and K. Hsu. 2016. "An in-Process Laser Localized pre-Deposition Heating Approach to Inter-Layer Bond Strengthening in Extrusion Based Polymer Additive Manufacturing." *Journal of Manufacturing Processes* 24: 179–185.

Ravoori, D., L. Alba, H. Prajapati, and A. Jain. 2018. "Investigation of Process-Structure-Property Relationships in Polymer Extrusion Based Additive Manufacturing Through *In situ* High Speed Imaging and Thermal Conductivity Measurements." *Additive Manufacturing* 23: 132–139.

Ravoori, D., C. Lowery, H. Prajapati, and A. Jain. 2019a. "Experimental and Theoretical Investigation of Heat Transfer in Platform Bed During Polymer Extrusion Based Additive Manufacturing." *Polymer Testing* 73: 439–446.

Ravoori, D., H. Prajapati, V. Talluru, A. Adnan, and A. Jain. 2019b. "Nozzle-integrated Pre-deposition and Post-deposition Heating of Previously Deposited Layers in Polymer Extrusion Based Additive Manufacturing." *Additive Manufacturing* 28: 719–726.

Rezaee, A., and A. Adnan. 2018. "On the Elastic Stress Singularities and Mode I Notch Stress Intensity Factor for 3D Printed Polymers." *Engineering Fracture Mechanics* 204: 235–245.

Seppala, J. E., S. H. Han, K. E. Hillgartner, C. S. Davis, and K. B. Migler. 2017. "Weld Formation During Material Extrusion Additive Manufacturing." *Soft Matter* 13: 6761–6769.

Sood, A. K., R. K. Ohdar, and S. S. Mahapatra. 2010. "Parametric Appraisal of Mechanical Property of Fused Deposition Modelling Processed Parts." *Materials & Design* 31: 287–295.

Sun, Q., G. M. Rizvi, C. T. Bellehumeur, and P. Gu. 2008. "Effect of Processing Conditions on the Bonding Quality of FDM Polymer Filaments." *Journal of Manufacturing Processes* 14: 72–80.

Sweeney, C., B. Lackey, M. Pospisil, T. Achee, V. Hicks, A. Moran, B. Teipel, M. Saed, and M. Green. 2017. "Welding of 3D-Printed Carbon Nanotube–Polymer Composites by Locally Induced Microwave Heating." *Science Advances* 6: 1–6.

Tymrak, B. M., M. Kreiger, and J. M. Pearce. 2014. "Mechanical Properties of Components Fabricated with Open-Source 3-D Printers Under Realistic Environmental Conditions." *Materials & Design* 58: 242–246.

Wittbrodt, B., and J. M. Pearce. 2015. "The Effects of PLA Color on Material Properties of 3-D Printed Components." *Additive Manufacturing* 8: 110–116.

Wong, K. V., and A. Hernandez. 2012. "A Review of Additive Manufacturing." *ISRN Mechanical Engineering* 1: 1–10.

Yang, F., and R. Pitchumani. 2002. "Interlaminar Contact Development During Thermoplastic Fusion Bonding." *Polymer Engineering & Science* 42: 424–438.

Zhao, X., H. Hu, X. Wang, X. Yu, W. Zhou, and S. Peng. 2020. "Super Tough Poly(Lactic Acid) Blends: a Comprehensive Review." *RSC Advances* 10: 13316–13368.